

Multi-label Image Classification using Adaptive Graph Convolutional Networks: from a Single Domain to Multiple Domains

Indel Pal Singh., *Member, IEEE*, Enjie Ghorbel, Oyebade Oyedotun, Djamila Aouada, *Senior member, IEEE*

arXiv:2301.04494v1 [cs.CV] 11 Jan 2023

Abstract—This paper proposes an adaptive graph-based approach for multi-label image classification. Graph-based methods have been largely exploited in the field of multi-label classification, given their ability to model label correlations. Specifically, their effectiveness has been proven not only when considering a single domain but also when taking into account multiple domains. However, the topology of the used graph is not optimal as it is pre-defined heuristically. In addition, consecutive Graph Convolutional Network (GCN) aggregations tend to destroy the feature similarity. To overcome these issues, an architecture for learning the graph connectivity in an end-to-end fashion is introduced. This is done by integrating an attention-based mechanism and a similarity-preserving strategy. The proposed framework is then extended to multiple domains using an adversarial training scheme. Numerous experiments are reported on well-known single-domain and multi-domain benchmarks. The results demonstrate that our approach outperforms the state-of-the-art in terms of mean Average Precision (mAP) and model size.

Index Terms—multi-label image classification, graph convolutional networks, attention mechanism, similarity-preserving strategy, domain adaptation.

I. INTRODUCTION

MULTI-label image classification has been widely investigated by the computer vision community. This popularity could be explained by its numerous fields of application such as human attribute recognition [3], multi-object recognition [5] and scene classification [4]. In contrast to traditional image classification approaches that attempt to associate a single label to a given image, multi-label image classification aims to detect the presence of a set of objects in an image.

Over the last years, the advancements in Deep Learning (DL) have significantly enhanced the performance of multi-label image classification [6], [7]. In general, these approaches can be divided into two main categories. The first category that we refer to as *direct methods* [6]–[8] is the most intuitive. The latter simply trains a single-stream deep neural network for performing multiple binary classification tasks. Nevertheless, these approaches often require a large number of layers to achieve high performance. Consequently, the number of parameters increases, resulting in very large networks that are hardly deployable in memory-constrained applications.

This work was funded by the Luxembourg National Research Fund (FNR), under the project reference BRIDGES2020/IS/14755859/MEETA/Aouada

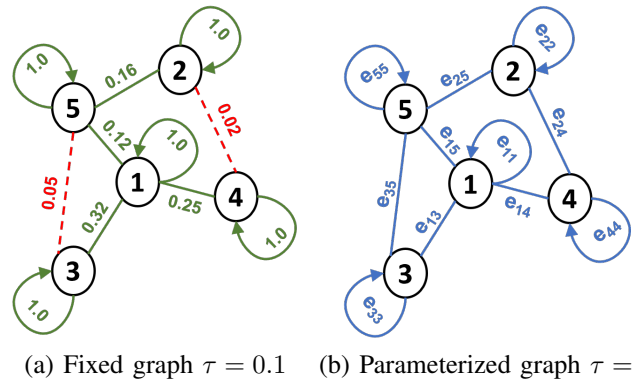


Fig. 1: (a) An example of a fixed label graph with a threshold set to $\tau = 0.1$. Dashed (red) edges indicate the ignored edges; (b) The proposed parameterized graph topology considering all the edges.

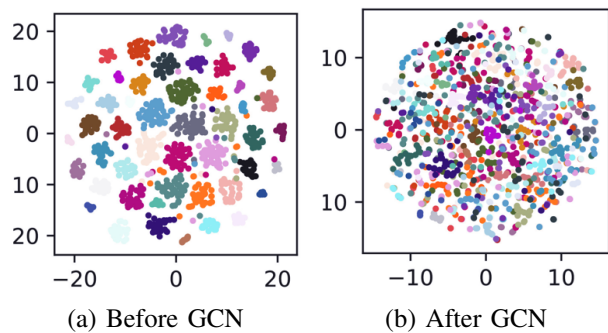


Fig. 2: Features of graph nodes: the similarity between the node features is lost after GCN aggregations.

As an alternative, *indirect methods* aim at leveraging the prior knowledge related to labels [9]–[11]; therefore resulting on more compact networks. Label correlations is an important cue. In fact, it is common sense that some objects are more likely to appear in the same image than others. For instance, a skateboard would appear more likely with a person than a dog. As demonstrated in [11] and [37], implicitly integrating the information of label correlation can be a solution for enhancing the network scalability while achieving a comparable performance to direct methods.

Graph-based approaches are among the most popular in-

direct methods [10], [11] given their ability to naturally model label correlations. These approaches have shown great performance in terms of both accuracy and network size. However, they are still limited from two different perspectives. The first challenge is proper to Graph Convolutional Network (GCN)-based methods [10], [11]. Indeed, these methods are negatively impacted by three observations: (1) The graph structure is heuristically defined. In general, a graph topology is represented by an adjacency matrix which is based on a label co-occurrence matrix that is computed using training data. Hence, this topology might not be ideal for the specific task of multi-label image classification; (2) A threshold is empirically fixed and used for discarding edges showing a low co-occurrence probability (see Fig. 1(a)). As a consequence, infrequent co-occurrences are regarded as noisy. While this often holds, it might not be correct in some cases; and (3) as shown in [14], successive aggregation operations in the GCN aggregation procedure usually alter the node representation similarity in the original feature space. As a result, this might be translated into a precision decrease. The second challenge is more general and concerns most multi-label classification techniques. They usually assume that unseen images and training data are drawn from the same distribution, hence ignoring a possible domain shift problem [22]. This leads, therefore, to poor generalization capabilities. Unsupervised domain adaptation is a plausible solution to overcome this issue without relying on costly annotation efforts [15]. It aims at learning domain invariant features to bridge the gap between a source domain and a target domain without access to the associated labels. While unsupervised domain adaptation has been widely investigated in the context of single-label image classification, very few works have considered this strategy for multi-label image classification [22], [23]. One of the most well-known domain adaptation-based multi-label classification frameworks [22] leverages graph representations to model label inter-dependencies and couple it with an adversarial training approach [19]. However, since it is a direct extension of [10], it naturally inherits from the same limitation mentioned earlier, e.g., (1) the heuristically defined structure of the graph, (2) an empirically set threshold, and (3) node feature dissimilarity.

In this paper, we propose an adaptive graph-based multi-label classification method called Multi-Label Adaptive Graph Convolutional Network (ML-AGCN) working effectively in both contexts, single domain and across domains. Our idea consists in: (1) learning two additional adjacency matrices in an end-to-end manner instead of solely relying on a heuristically defined graph topology as illustrated in Fig. 1. Note that no threshold is applied, avoiding the loss of weak yet relevant connections. In particular, the first learned graph topology computes the importance of each node pair. This is carried out by employing an attention mechanism similar to Graph Attention Networks (GAT) [32]. The second one is built based on the similarity between node features and overcomes the information loss happening through successive convolutions; (2) integrating the proposed adaptive graph-based architecture in an adversarial domain adaptation framework for aligning a source domain to an unlabeled target domain. The results

suggest that our method is competitive with respect to the state-of-the-art while being more compact i.e. requiring a smaller number of parameters in both cases (single domain and across domains).

This paper is an extended version of [41]. In comparison to [41], the main contributions of this article are given below:

- 1) An adversarial domain adaptation approach integrating an adaptive graph convolutional network for multi-label image classification.
- 2) More extensive experiments and analyses showing the relevance of the proposed architecture called Multi-Label Adaptive Graph Convolutional Network (ML-AGCN) for multi-label image classification.
- 3) A deep qualitative and quantitative experimental analysis of the proposed domain adaptation method with respect to the state-of-the-art.

The remainder of this paper is organized as follows. Section II reviews the state-of-the-art on multi-label image classification and domain adaptation for multi-label classification. Section III formulates the problem of graph-based multi-label image classification and its applicability to different domains. In Section IV and V, the proposed method is detailed. Section VI presents the experimental results and analysis. Finally, Section VII concludes this work and highlights interesting future directions.

II. RELATED WORKS

In this section, we start by presenting the state-of-the-art of multi-label image classification. Then, we focus on reviewing existing domain adaptation approaches for multi-label image classification.

A. Multi-label Image Classification

As discussed in Section I, two paradigms exist in the literature for handling the problem of multi-label image classification. On the one hand, the direct one [6]–[8] aims to learn a single stream deep convolutional neural network (CNN) for carrying out multiple binary classifications, where each classifier is associated with one label. Direct methods take mostly inspiration from successful architectures proposed in the context of single-label image classification. For example, Razavian et al. [51] have used a pre-trained OVERFeat [52] model and have adapted it to multi-label image classification. Wei et al. [47] have leveraged the prediction of multiple CNN architectures pretrained on ImageNet [48] such as AlexNet [53] and VGG-16 [54]. Ridnik et al. [24] have employed TResNet [6] using a novel loss called Asymmetric Loss (ASL) that focuses more on positive samples than negative ones. TResNet introduced in [6] is based on a ResNet architecture with a series of modifications for optimizing the GPU network capabilities while maintaining the performance. Recently, Lanchantin et al. [37] attempted to leverage transformers for modeling complex dependencies among visual features and labels.

Going deeper into the network enables the model to learn more abstract features from the image. However, this comes at the cost of high memory requirements. Moreover, direct

methods do not explicitly model the relationship between labels which can be an important semantic element to consider.

In order to incorporate the information of label correlations, *indirect* methods generally use a second subnetwork in addition to the main backbone. For instance, Zhu et al. [49] have introduced a Spatial Regularization Net (SRN) to learn the underlying relationships between labels by generating label-wise attention maps. Similarly, Qu et al. [58] have employed image representations from intermediate convolutional layers to model both local and global label semantics.

Graphs can also be an interesting way for modeling label correlations [9]–[11], while keeping the network size reasonable. Graph-based methods [9]–[11] usually employ a GCN for learning interdependent label-wise classifiers and combine it with a CNN that learns discriminative image features. The input graph is heuristically predefined based on label co-occurrences in the training set, where low values are ignored. However, following such an empirical strategy might lead to sub-optimal performances. Additionally, destroying the similarity of node features through the GCN layers might lead to a decrease in performance, as discussed in [14].

B. Domain Adaptation

Over the last years, DL methods have achieved a remarkable progress in the field of computer vision and pattern recognition. However, the effectiveness of DL approaches heavily depends on the availability of a large amount of annotated data. For mitigating the huge cost caused by data annotation, the field of unsupervised domain adaptation [16]–[20] has been widely investigated over the last decade. It aims at making use of an existing labeled dataset from a related domain called *source domain* to enhance the model performance on a domain of interest termed *target domain*, for which only unlabeled data are provided.

Unsupervised domain adaptation methods can be separated into two main categories. The first one [16]–[18] aims at explicitly reducing the domain gap by minimizing statistical discrepancy measures between the two domains. Alternatively, the second class of methods implicitly minimizes this domain gap by adopting an adversarial training approach [19], [20]. The main idea consists in using a domain classifier to play a min-max two-player game with the feature generator. This strategy is designed to enforce the generation of domain-invariant features that are sufficiently discriminative.

Nevertheless, most existing techniques focus on the task of single-label image classification. In fact, very few papers have considered domain adaptation for multi-label image classification [10], [55], [57].

Among these rare references, we can mention ML-ANet [57], which explicitly minimizes the domain gap by optimizing multi-kernels maximum mean discrepancies (MK-MMD) in a Reproducing Kernel Hilbert Space (RKHS). More recently, an adversarial approach has been adopted in [55] where a condition-based domain discriminator similar to conditional-GANs [56] has been employed. However, similar to direct methods for traditional multi-label image classification, these two approaches [55], [57] neglect the

important information of label dependencies. A graph-based approach called DA-MAIC has been then proposed as an alternative [22]. As in ML-GCN [10], they have proposed to build a graph for modeling label correlations based on label co-occurrences. Additionally, to reduce the domain shift between the source and target domains, they have used a domain classifier that is trained in an adversarial manner. Unfortunately, DA-MAIC is impacted by the same drawbacks affecting ML-GCN [10] as detailed in Section I. More details regarding these issues are given in the next section.

III. BACKGROUND AND PROBLEM FORMULATION

In this section, Graph Convolutional Networks (GCN) are first reviewed. Then, the two problems of multi-label image classification and unsupervised domain adaptation for multi-label image classification are formulated.

A. Background: Graph Convolutional Networks (GCN)

CNNs are defined on a regular grid and are, therefore, not directly applicable to non-Euclidean structures such as graphs. GCN [50] has been proposed as the generalization of traditional CNN to graphs. They have been very successful in numerous computer vision applications, including human pose estimation [2] and human action recognition [1]. Let us denote a graph by $G = (V, E, \mathbf{F})$ where $V = \{v_1, v_2, \dots, v_N\}$ corresponds to the set of N nodes and $E = \{e_1, e_2, \dots, e_M\}$ refers to the set of M edges connecting the nodes and $\mathbf{F} = \{\mathbf{f}_1, \mathbf{f}_2, \dots, \mathbf{f}_N\}$ represents the node features such that $\mathbf{f}_i \in \mathbb{R}^d$ corresponds to the features of the node v_i .

Let us assume that \mathbf{F}^l is the input node features of the l^{th} layer and $\mathbf{A} \in \mathbb{R}^{N \times N}$ the adjacency matrix of the graph \mathcal{G} . Each GCN layer can be seen as a non-linear function $h(\cdot)$ that computes the node features $\mathbf{F}^{l+1} \in \mathbb{R}^{N \times d'}$ of the $(l+1)^{\text{th}}$ layer as follows,

$$\mathbf{F}^{l+1} = h(\mathbf{A}\mathbf{F}^l\mathbf{W}^l), \quad (1)$$

where $\mathbf{W}^l \in \mathbb{R}^{d \times d'}$ is the weight matrix. Note that \mathbf{A} is normalized before using Eq. (1).

B. Problem formulation

1) *Graph-based multi-label image classification*: The goal of multi-label image classification is to predict the presence or absence of a set of objects $\mathcal{O} = \{1, 2, \dots, N\}$ in a given image \mathbf{I} . This can be done by learning a function f such that,

$$f: \mathbb{R}^{w \times h} \rightarrow \llbracket 0, 1 \rrbracket^N$$

$$\mathbf{I} \mapsto \mathbf{y} = [y_i]_{i \in \mathcal{O}},$$

where w and h define the pixel-wise width and height of the image, respectively. $y_i = 1$ indicates the presence of the label i in \mathbf{I} , in contrast to $y_i = 0$. Graph-based multi-label image classification methods such as ML-GCN [10] and IML-GCN [11] usually involve two subnetworks: (1) A feature generator denoted by f_g , and (2) an estimator of N inter-dependent binary classifiers denoted by f_c . The generator mostly corresponds to an out-of-the-shelf CNN network

which produces a d_f -dimensional image feature representation as described below.

$$\begin{aligned} f_g: \mathbb{R}^{w \times h} &\rightarrow \mathbb{R}^{d_f} \\ \mathbf{I} &\mapsto \mathbf{X}. \end{aligned} \quad (2)$$

For instance, ML-GCN [10] integrates a ResNet101 [7], while IML-GCN makes use of TResNet [6].

On the other hand, the second subnetwork f_c is a GCN formed by L layers which takes a fixed graph $G = (V, E, \mathbf{F})$ as input where $\text{card}(V) = N$. In fact, each node $v_i \in V$ refers to the label $i \in \{1, 2, \dots, N\}$ and each $\mathbf{f}_i \in \mathbf{F}$ corresponds to its associated label embedding. The adjacency matrix $\mathbf{A} \in \mathbb{R}^{N \times N}$ of G is usually pre-computed based on the co-occurrence probabilities that are estimated over the training set [10], [11]. In addition, rare co-occurrences are discarded as they are assumed to be noisy. In other words, given an empirically fixed threshold τ ,

$$\mathbf{A}_{ij} = \begin{cases} 0, & \text{if } p_{ij} < \tau, \\ 1, & \text{if } p_{ij} \geq \tau \end{cases}, \quad (3)$$

such that $p_{ij} = p(I_j | I_i)$ is the co-occurrence probability that the label j is present given that the label i is already known to be in a given image.

Given $\mathbf{F}^l \in \mathbb{R}^{d_l \times L}$ as the input node features of the l^{th} layer, the input features \mathbf{F}^{l+1} of the $(l+1)^{\text{th}}$ are therefore computed by following Eq. (1).

Finally, the vertex features produced by the last GCN layer, i.e., $\mathbf{F}^L \in \mathbb{R}^{N \times d_f}$, form the N inter-dependent classifiers.

In summary, f_c can be defined as follows,

$$\begin{aligned} f_c: \mathcal{G}(N) &\rightarrow \mathbb{R}^{d_f \times N} \\ G &\mapsto \mathbf{F}^L = [F_1^L, \dots, F_N^L], \end{aligned} \quad (4)$$

where $\mathcal{G}(N)$ represents the set of graphs with N nodes and \mathbf{F}_i^L for $i \in \{1, \dots, N\}$ is the generated inter-dependent binary classifier associated to the label i .

Hence, f , which returns the final prediction, can be defined as follows,

$$\begin{aligned} f(\mathbf{I}) &= \text{sig}(f_c(G)f_g(\mathbf{I})^T) \\ &= \text{sig}(\mathbf{F}^L \mathbf{X}^T), \end{aligned} \quad (5)$$

where $\text{sig}(x) = \frac{1}{1+e^{-x}}$ is the sigmoid activation function.

However, as explained in Section I, three main limitations can be noted: (1) the computation of the adjacency matrix \mathbf{A} is made heuristically and is completely decoupled from the training process; (2) a threshold is empirically fixed for completely ignoring rare co-occurrences; and (3) as shown in [14], aggregating successively node features in a graph may induce the loss of the similarity/dissimilarity information present in the initial feature space.

C. Graph-based unsupervised domain adaptation for multi-label image classification

Let us consider a source dataset for multi-label image classification $\{(\mathbf{I}_s^k, \mathbf{y}_s^k)\}_{k=1}^{n_s}$ drawn from a distribution \mathcal{D}_s and a similar unlabelled target dataset $\{(\mathbf{I}_t^k)\}_{k=1}^{n_t}$ drawn from a

different distribution \mathcal{D}_t . $\mathbf{I}_s^k \in \mathbb{R}^{w \times h}$ refers to the k^{th} image sample of \mathcal{D}_s and $\mathbf{y}_s^k \in \{0, 1\}^N$ is its associated label vector, while $\mathbf{I}_t^k \in \mathbb{R}^{w \times h}$ denotes the k^{th} image sample of \mathcal{D}_t . n_s and n_t refer respectively the total number of samples in \mathcal{D}_s and \mathcal{D}_t . The goal of unsupervised domain adaptation is to train a model using labeled source domain data sampled from \mathcal{D}_s and unlabelled target domain samples from \mathcal{D}_t for making accurate predictions on the target domain. Despite its relevance in real-world applications, few domain adaptation methods have been proposed for multi-label image classification. Among the most recent and accurate approaches, one can mention DA-MAIC [22], which also takes advantage of the graph representation for modeling label correlations. It directly extends ML-GCN [10] by integrating an adversarial training for domain adaptation. Consequently, DA-MAIC is subject to the same limitations induced by ML-GCN [10] mentioned in Section III-B1.

IV. MULTI-LABEL ADAPTIVE GRAPH CONVOLUTIONAL NETWORK (ML-AGCN)

To handle the challenges mentioned in Section III, a novel graph-based approach called Multi-Label Adaptive Graph Convolutional Network (ML-AGCN) is introduced.

A. Overview of the proposed architecture

Similar to [10] and [11], a network formed by two subnets is adopted as illustrated in Fig 3. The first is a CNN that extracts a discriminative representation from a given input image, while the second is a GCN-based network that learns N interdependent classifiers. As in [11], TResNet-M which represents a small version of TResNet [6] is employed as a CNN subnetwork. TResNet is a direct extension of ResNet, which fully exploits the GPU capabilities to boost the model efficiency. The graph-based subnet, Adaptive Graph Convolutional Network (AGCN), uses the same image embeddings proposed in [11] as feature nodes. Nevertheless, in contrast to [11] and [10], it relies on an end-to-end learned graph topology. More details regarding this subnetwork are provided in Section IV-B. Similar to [11], the Asymmetric Loss (ASL) [24] denoted by \mathcal{L}_c is used for optimizing ML-AGCN such that,

$$\begin{aligned} \mathcal{L}_c &= \mathbb{E}_{(\mathbf{I}_s, \mathbf{y}_s) \sim \mathcal{D}_s} \sum_{i=1}^N y_s^{(i)} (1 - p^{(i)})^{\gamma_+} \log(p^{(i)}) + \\ &\quad (1 - y_s^{(i)}) (p_m^{(i)})^{\gamma_-} \log(1 - p_m^{(i)}), \end{aligned} \quad (6)$$

where γ_+ and γ_- are focusing parameters for positive and negative samples, respectively, and $y_s^{(i)}$ and $p^{(i)}$ are the respective ground truth and predicted probability for the label i . $p_m^{(i)}$ is the shifted probability, given by $\max(p^{(i)} - m, 0)$, where m is a threshold to diminish the effect of easy negative samples [24].

B. Graph-based subnet: Adaptive Graph Convolutional Network (AGCN)

Our intuition is that by integrating a suitable mechanism, it should be possible to boost the classification performance

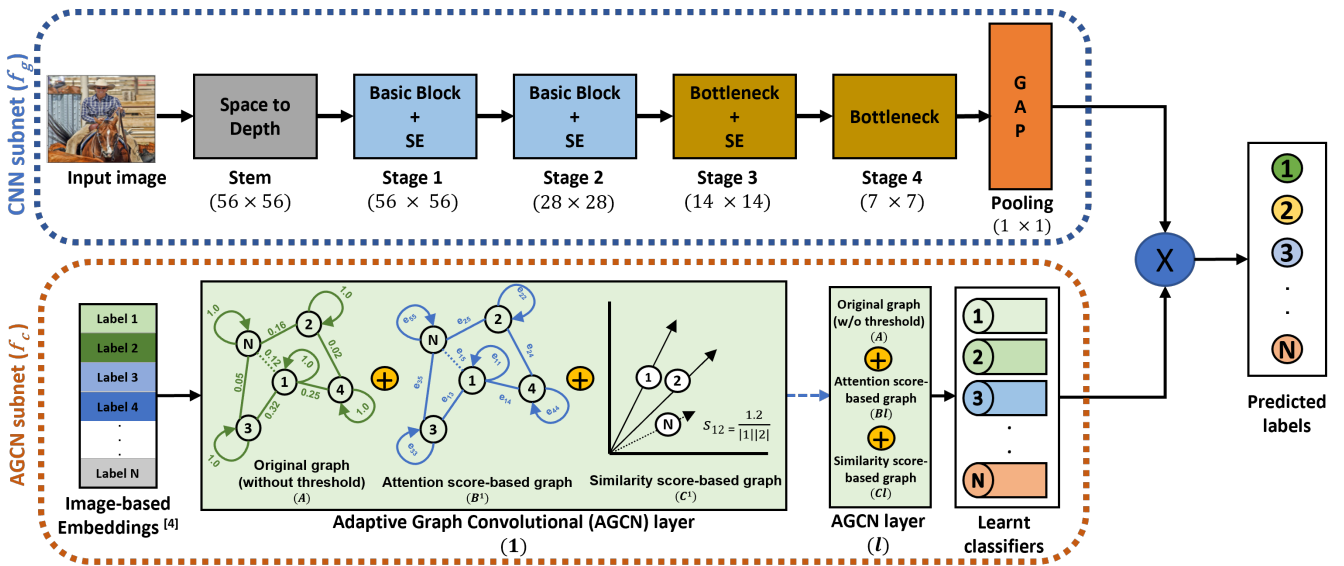


Fig. 3: Architecture of ML-AGCN: On the one hand, the CNN subnet learns relevant image features from an input image. On the other hand, the GCN-subnet estimates interdependent label classifiers by taking into account one fixed adjacency matrix \mathbf{A} and two adaptive adjacency matrices $\mathbf{B}^{(l)}$ and $\mathbf{C}^{(l)}$. Finally, the classifiers are applied to the CNN features for predicting the labels.

and reduce at the same time the size of graph-based methods. Hence, we propose to adaptively learn the graph topology by reformulating Eq. (1) as below,

$$\mathbf{F}^{l+1} = \sigma((\mathbf{A} + \mathbf{B}^{(l)} + \mathbf{C}^{(l)})\mathbf{F}^l\mathbf{W}^l), \quad (7)$$

where σ is a LeakyRELU activation function.

Instead of relying solely on the adjacency matrix \mathbf{A} defined in [10], two additional parameterized graph topologies called attention-based and similarity adjacency graphs, respectively denoted by $\mathbf{B}^{(l)}$ and $\mathbf{C}^{(l)}$, are defined. In this case, no threshold is applied to \mathbf{A} for ignoring rare co-occurrences. It is also important to remark that \mathbf{A} is fixed, while $\mathbf{B}^{(l)}$ and $\mathbf{C}^{(l)}$ vary from one layer to another. In the following, we detail how $\mathbf{B}^{(l)}$ and $\mathbf{C}^{(l)}$ are computed.

1) *Attention-based adjacency matrix*: Instead of ignoring rare co-occurrences in \mathbf{A} , the matrix $\mathbf{B}^{(l)} = (b_{ij}^{(l)})_{i,j \in \mathcal{O}}$ is defined based on an attention mechanism where the importance of each edge is quantified. To that aim, inspired by [32], an attention score denoted by e_{ij} is calculated for each pair of vertices (v_i, v_j) as follows,

$$e_{ij} = \sigma(\mathbf{a}^{(l)T} (\mathbf{W}\mathbf{F}_i^{(l)} \parallel \mathbf{W}\mathbf{F}_j^{(l)})), \quad (8)$$

where $\mathbf{W} \in \mathbb{R}^{d^{(l+1)} \times d^{(l)}}$ represents a learnable weight matrix and $\mathbf{a}^{(l)T} \in \mathbb{R}^{2d^{(l+1)}}$ are the learnable attention coefficients. \parallel refers to the concatenation operation.

A softmax function is then applied to the computed normalized attention scores such that,

$$\alpha_{ij}^{(l)} = \frac{\exp(e_{ij}^{(l)})}{\sum_{k \in \mathcal{N}(i)} \exp(e_{ik}^{(l)})}, \quad (9)$$

with $\mathcal{N}(i)$ defining the neighborhood of the node i and α_{ij} being the obtained normalized attention score.

We recall that the goal of the GCN subnet is to generate interdependent label classifiers. This means that each classifier must be predominated by the information related to the label it belongs to. Hence, the attention score of the node in question should be maximal. For this purpose, an additional step called self-importance mechanism is proposed and allows computing the attention-based adjacency matrix $\mathbf{B}^{(l)} = (b_{ij}^{(l)})_{i,j \in \mathcal{O}}$ as follows,

$$\begin{cases} b_{ij}^{(l)} = \alpha_{ij}^{(l)} + \max_{k \in \mathcal{O}} (\alpha_{ik}^{(l)}) & \text{if } i = j \\ b_{ij}^{(l)} = \alpha_{ij}^{(l)} & \text{if } i \neq j \end{cases}. \quad (10)$$

2) *Similarity-based adjacency matrix (C)*: As discussed in Section I, the GCN aggregation tends to modify the node similarity in the original feature space [14]. To overcome this issue, a node-similarity preserving matrix $\mathbf{C}^{(l)} = (c_{ij}^{(l)})_{i,j \in \mathcal{O}}$ is proposed. It is obtained by calculating the cosine similarity $c_{ij}^{(l)}$ between each pair of vertices (v_i, v_j) as follows,

$$c_{ij}^{(l)} = \frac{\mathbf{F}_i^{(l)} \cdot \mathbf{F}_j^{(l)}}{\|\mathbf{F}_i^{(l)}\| \|\mathbf{F}_j^{(l)}\|}, \quad (11)$$

where $\|\cdot\|$ denotes the L_2 Euclidean norm.

Finally, the output of the final layer L denoted by \mathbf{F}^L is used in Eq. (5) for predicting the labels.

V. DOMAIN ADAPTATION FOR MULTI-LABEL IMAGE CLASSIFICATION USING ML-AGCN

The overall architecture of the proposed domain adaptation method called DA-AGCN for multi-label image classification is shown in Fig. 4. Similar to ML-AGCN, we make use of TRResNet-based f_g to extract discriminative image features and an Adaptive Graph Convolutional Network f_c to learn N interdependent classifiers. Given source and target input

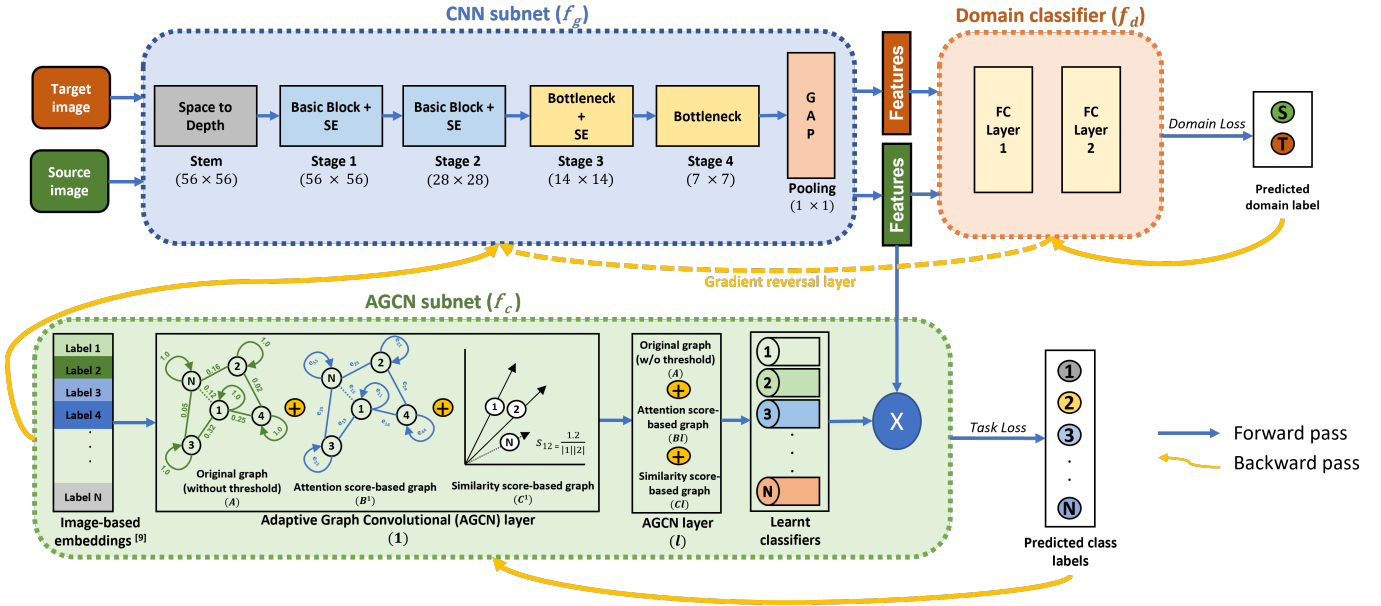


Fig. 4: Architecture of the proposed AGCN-based domain adaptation method for multi-label image classification (best viewed in color). Images from both source and target datasets are given as input to the CNN subnet that generates image features. The AGCN-subnet learns in an end-to-end manner the attention and similarity-based adjacency matrices $\mathbf{B}^{(l)}$ and $\mathbf{C}^{(l)}$, respectively, and generates accordingly inter-dependent label classifiers using only labeled source images. In addition, a domain classifier is considered.

images from \mathcal{D}_s and \mathcal{D}_t , respectively, the goal of f_g is to generate D -dim domain-invariant image features. The latter is used to predict the image labels, as depicted in Eq. (5). The label classification loss \mathcal{L}_c is therefore defined as in Eq. (6). For obtaining domain-invariant representations, a domain classifier $f_d: \mathbb{R}^{d_f} \rightarrow \llbracket 0, 1 \rrbracket$ is employed and trained in an adversarial manner. Given the features $\mathbf{X} = f_g(\mathbf{I})$ extracted from a given image \mathbf{I} , f_d predicts the domain of the input image as follows,

$$f_d: \mathbb{R}^{d_f} \rightarrow \llbracket 0, 1 \rrbracket$$

$$\mathbf{X} \mapsto \hat{d}. \quad (12)$$

where \hat{d} is the predicted domain label of \mathbf{I} . Note that the ground-truth domain label $d = 0$ if \mathbf{I} is from the source domain and $d = 1$ if sampled from the target domain.

As in [19], a domain loss is defined as below,

$$\mathcal{L}_d = \mathbb{E}_{f_g(\mathbf{I}_s) \sim \mathcal{D}_s} \log \frac{1}{f_d(f_g(\mathbf{I}_s))} +$$

$$\mathbb{E}_{f_g(\mathbf{I}_t) \sim \mathcal{D}_t} \log \frac{1}{(1 - f_d(f_g(\mathbf{I}_t)))}, \quad (13)$$

Given \mathcal{L}_c defined in Eq. (6), the final objective function used to optimize the network is $E(\theta_g, \theta_d, \theta_c)$ defined by,

$$E(\theta_g, \theta_d, \theta_c) = \mathcal{L}_c(\theta_c, \theta_g) + \lambda \mathcal{L}_d(\theta_d, \theta_g), \quad (14)$$

where θ_g, θ_d and θ_c refer respectively to the parameters of f_g, f_d and f_c and λ is a hyper-parameter defining the weight of \mathcal{L}_d . The network is trained in an adversarial manner for obtaining the optimal parameters $(\hat{\theta}_g, \hat{\theta}_c, \hat{\theta}_d)$ such that,

$$(\hat{\theta}_g, \hat{\theta}_c) = \min_{\theta_g, \theta_c} E(\theta_g, \theta_c, \hat{\theta}_d),$$

$$\hat{\theta}_d = \max_{\theta_d} E(\hat{\theta}_g, \hat{\theta}_c, \theta_d). \quad (15)$$

For that purpose, a reversal gradient layer is used as in [19].

VI. EXPERIMENTS

In this section, the experimental settings and results are presented and discussed for: (1) single-domain multi-label image classification (Section VI-A1); and (2) domain-adaptation for multi-label image classification (Section VI-B).

A. Multi-label Image Classification

1) *Implementation details:* As discussed in Section IV, TRResNet-M [6] is used as the CNN backbone. In particular, the fully connected layer after the Global Average Pooling (GAP) layer is removed. The output of the GAP layer produces a 2048-dimensional latent image representation. The dimension of the AGCN output has also been set to 2048. For the node features, we use the image-based embeddings proposed in [11] instead of the usual word-based embeddings used in [10]. The model is trained for 40 epochs using *Adam*, with a maximum learning rate of $1e-4$ using a cosine decay.

2) *Datasets:* In the following, the datasets that have been used for the experiments are presented.

a) *MS-COCO:* MS-COCO [33] is a widely used large-scale multi-label image dataset. It contains 80K training images and 40k testing images. Each image is annotated with multiple object labels from a total of 80 categories.

b) *VG-500*: The VG-500 dataset [35] is a well-known dataset for multi-label image classification. It includes 500 different objects as categories are used. The dataset comes with a training set of 98,249 images and a testing set of 10,000 images.

c) *PASCAL-VOC 2007*: The PASCAL Visual Object Classes Challenge [36] introduced in 2007 is one of the most commonly used multi-label image classification datasets. It contains about 10K image samples with 5011 and 4952 images as training and testing sets, respectively. The images show 20 different object categories with an average of 2.5 categories per image.

3) *Quantitative analysis*:

a) *Comparison with state-of-the-art methods in terms of mAP and model size*: We compare the performance of the proposed ML-AGCN with current state-of-the-art methods by reporting the mean Average Precision (mAP) as well as the number of model parameters. Additionally, similar to [10], [11], we report the following evaluation metrics on the MS-COCO dataset, namely, average per-Class Precision (CP), average per-Class Recall (CR), average per-Class F1-score (CF1), the average Overall Precision (OP), average overall recall (OR) and average Overall F1-score (OF1).

Table I, II and III reports the quantitative comparison of the proposed approach with state-of-the-art methods on the MS-COCO, the VG-500 and the VOC datasets, respectively. It can be clearly seen that our method outperforms existing methods in terms of mAP while considerably reducing the model size. More specifically, it achieves an improvement of respectively 0.3%, 3.4%, and 0.4% on MS-COCO, VG-500, and VOC-2007 as compared to the best-performing state-of-the-art methods. This is worth mentioning that ML-AGCN outperforms the ML-GCN [10] baseline by 3.9%, 6.3%, and 0.5% in terms of mAP while keeping a comparable number of parameters.

In addition, we also report that the obtained performance when including only one layer in the graph-subnet of ML-GCN [10], IML-GCN [11] and ML-AGCN). The obtained results confirm the relevance of the proposed adaptive learning. In fact, it can be seen that our method outperforms existing graph-based methods under this setting. More specifically, ML-AGCN achieves an improvement of 5.7% and 5.3% in terms of mAP when compared to ML-GCN and IML-GCN, respectively, on the MS-COCO dataset. Similarly, on the VG-500 benchmark, a significant increase of 20.7% is recorded in terms of mAP in comparison to IML-GCN.

b) *Ablation study*: In order to analyze the impact of each adjacency matrix used in our approach, namely, the attention-based matrix **B** and similarity-based matrix **C**, an ablation study is carried out as shown in Table IV. It can be noted that by considering **B** in addition to **A** (without threshold), an improvement of 5.1%, 20.5%, and 0.04% in terms of mAP is made, respectively, on MS-COCO, VG-500, and VOC-2007. An additional mAP improvement of 0.1%, 0.4%, and 0.17% can be seen when including **C** in the AGCN subnet. In conclusion, it can be remarked that **B** contributes more importantly to the resulting enhancement. This could be explained by the fact that **C** is less needed, as only two layers

are considered in the graph subnet. This would mean that the initial feature similarity is not completely lost through layers.

4) *Qualitative analysis*: In Fig. 5, the Gradient-weighted Class Activation Mapping (Grad-CAM) [42] is visualized for some examples from the VOC dataset. While the first column of images represents the input images, the second, third, and fourth columns show, respectively, the Grad-cam visualization from a model trained using only **A**, **A** and **B**, and finally **A**, **B** and **C**. These qualitative results are in line with the quantitative ones. As shown in Fig. 5, the use of **B** allows activating more precisely the regions of interest in the image, while the contribution of **C** in this refinement is less impressive but remains visible.

B. Domain Adaptation for Multi-label Image Classification

1) *Implementation details*: The same CNN backbone, namely, TRResNet is used. The domain classifier includes two successive MLP layers of dimension. A maximum learning rate of $1e-4$ using a cosine decay is considered. The model is trained for a total of 80 epochs.

2) *Datasets*:

a) *AID multi-label aerial dataset*: The original AID dataset [25] was introduced for the purpose of multi-class aerial scene classification. It contains 10000 high-resolution aerial images collected from worldwide Google Earth imagery, including scenes from China, the United States, England, France, Italy, Japan, and Germany. The images cover a total of 30 categories. The spatial resolution of the images varies from 0.5 m/pixel to 8 m/pixel, and the size of each aerial image is 600×600 pixels. A multi-label version of this dataset was produced in [26], where 3000 aerial images from the original AID dataset have been selected and assigned with multiple object labels. In total, they include 17 labels: airplane, sand, pavement, buildings, cars, chaparral, court, trees, dock, tank, water, grass, mobile-home, ship, bare-soil, sea, and field. 80% and 20% of the images have been used respectively for training and testing [26].

b) *UCM multi-label aerial dataset*: UCM multi-label dataset [27] is derived from the UCM dataset [28]. It consists of images showing 21 land-use classes selected from aerial orthoimagery. The images have a resolution of 256×256 pixels. Most of the images were downloaded from the United States Geological Survey (USGS). Later in [27], 2100 of these aerial images were annotated with multiple tags in order to generate a multi-label aerial image dataset. This dataset shares the same number of labels as AID multi-label dataset [26] i.e., total 17 labels. In our experiments, 80% and 20% of data are respectively used for training and testing.

c) *DFC15 multi-label aerial dataset*: The DFC15 multi-label dataset [29] was initially introduced in 2015. It has a total of 3342 high-resolution image samples and includes 8 object labels: impervious, water, clutter, vegetation, building, tree, boat, and car. In our experiments, the 6 categories in common with UCM and AID datasets, including water, grass, building, tree, ship, and car, are considered. 80% and 20% are respectively used for training and testing.

3) *Quantitative analysis*:

TABLE I: Comparison with the state-of-the-art methods in terms of mean Average Precision (mAP) and number of model parameters on the MS-COCO dataset.(Best performance is indicated in bold).

Method	# params (millions)	mAP	CP	CR	CF1	OP	OR	OF1
CNN-RNN [39]	66.2 M	61.2	-	-	-	-	-	-
ResNet101 [7]	44.5M	77.3	80.2	66.7	72.8	83.9	70.8	76.8
Multi-Evidence [40]	~47M	-	80.4	70.2	74.9	85.2	72.5	78.4
ML-GCN (2-layers) [10]	44.9M	83	85.1	72	78	85.8	75.4	80.3
ML-GCN (1-layer)* [†] [10]	43.1	80.9	82.9	69.7	75.8	84.8	73.6	78.8
SSGRL [38]	92.2M	83.8	89.9	68.5	76.8	91.3	70.8	79.7
KGGR [35]	~45M	84.3	85.6	72.7	78.6	87.1	75.6	80.9
C-Tran [37]	120M	85.1	86.3	74.3	79.9	87.7	76.5	81.7
ASL (TResNetM) [24]	29.5M	81.8	82.1	72.6	76.4	83.1	76.1	79.4
ASL (TResNetL) [24]	53.8M	86.6	87.4	76.4	81.4	88.1	79.2	81.8
IML-GCN (2-layers) [11]	31.5M	86.6	78.8	82.6	80.2	79.0	85.1	81.9
IML-GCN (1-layer)* [†] [11]	29.5M	81.3	81.3	72.2	76.0	86.7	77.9	82.1
Ours: ML-AGCN (2-layers)	35.9M	86.9	86.2	78.3	81.7	87.2	80.7	83.8
Ours: ML-AGCN (1-layer)*	29.9M	86.6	79.6	82.4	80.7	79.8	84.5	82.1

*Graph-based approaches within 1-layer GCN setting

[†]Reproduced results

TABLE II: Comparison with the state-of-the-art methods in terms of mean average precision (mAP) and number of model parameters on the VG-500 dataset.(Best performance is indicated in bold).

Method	# params (millions)	mAP (%)
ResNet-101 [7]	44.5	30.9
ML-GCN [10]	44.9	32.6
ASL (TResNetM) [†] [24]	29.5	33.6
ASL (TResNetL) [†] [24]	54.8	34.7
C-Tran [37] [‡]	120 [‡]	38.4 [‡]
IML-GCN (2-layers) [11])	32.1	34.5
IML-GCN (1-layer) ^{†*} [11])	30.6	17.2 ^{†*}
Ours: ML-AGCN (2-layers)	37.4	37.1
Ours: ML-AGCN (1-layer)*	32.7	37.9*

[‡]The model is roughly 250% larger than our proposal

*Graph-based approaches within 1-layer GCN setting

[†]Reproduced results

TABLE III: Comparison with the state-of-the-art methods in terms of mean average precision (mAP) and number of model parameters on the VOC-2007 dataset.(Best performance is indicated in bold).

Method	# params (millions)	mAP (%)
CNN-RNN [39]	66.2	84.0
ML-GCN (1-layer)* [†] [10]	43.1	88.9
ResNet-101 [7]	44.5	89.9
ASL (TResNet-M) [24]	29.5	91.1
IML-GCN [11]	33.5	91.9
IML-GCN (PCA) [11]	31.4	92.1
SSGRL [38]	92.2	93.4
ML-GCN [10]	44.9	94.0
ASL (TResNet-L) [24]	53.8	94.6
Ours: ML-AGCN (2-layers)	35.7	95.0
Ours: ML-AGCN (1-layer)*	29.5	94.5*

*Graph-based approaches within 1-layer GCN setting

[†]Reproduced results

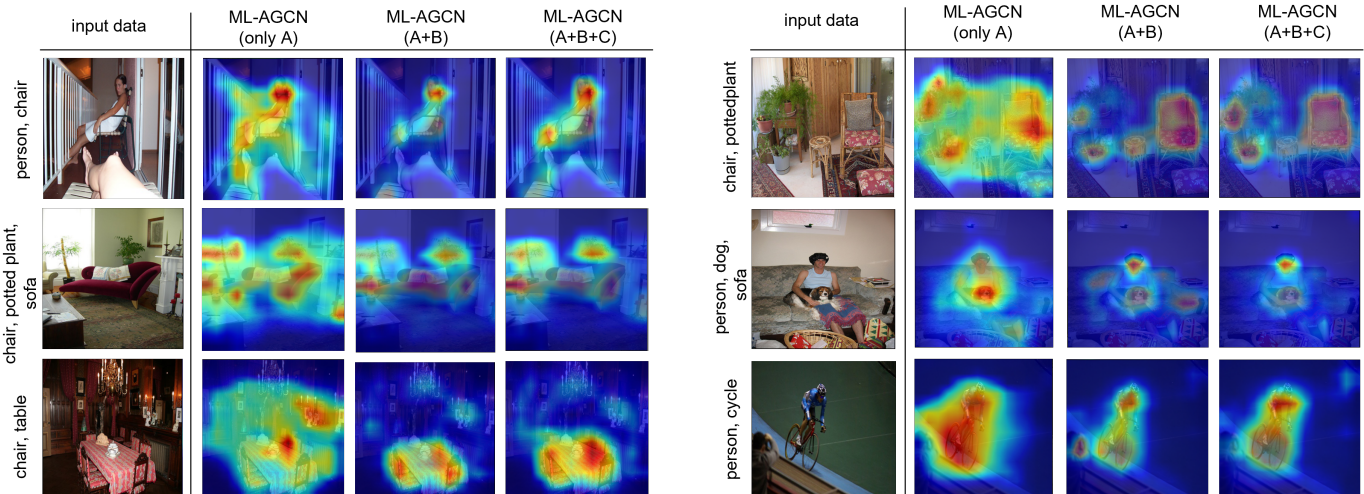


Fig. 5: Grad-CAM visualization of the predictions using samples from the VOC dataset using only A, then A and B, and finally A, B and C.

a) Comparison with state-of-the-art methods in terms of mAP and model size: The proposed domain adaptation approach for multi-label image classification approach is

compared with state-of-the-art methods. The same metrics described in Section VI-A3 are used, including mAP, CP, CR, CF1, OP, OR and OF1. As in DA-MAIC [22], four

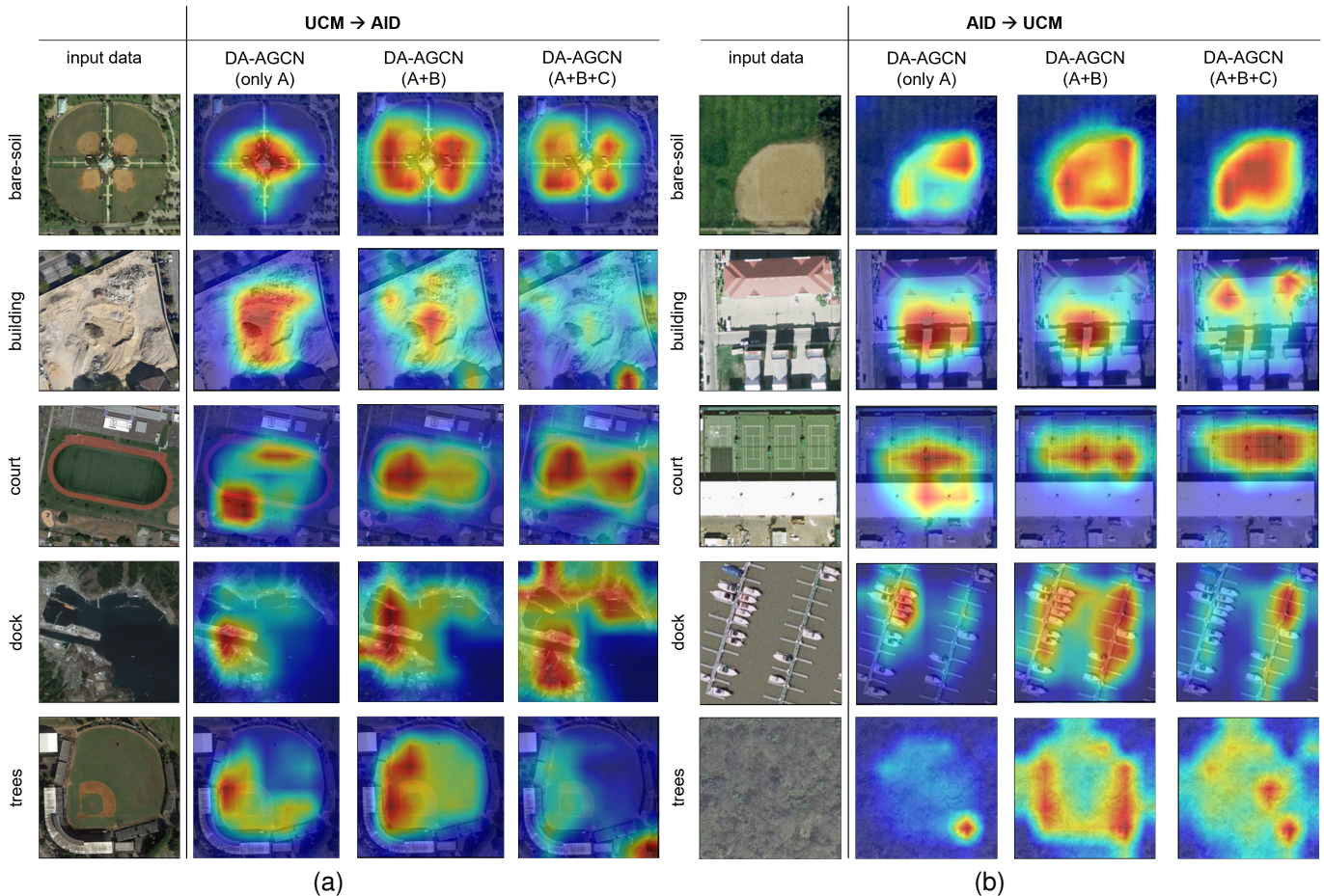


Fig. 6: Grad-CAM visualization of the predictions a) UCM \rightarrow AID, and b) AID \rightarrow UCM setting using only A, then A and B, and finally A, B and C.

TABLE IV: The ablation of adaptively learning B and C) for multi-label image classification.

Methods/Dataset (mAP %)	MS-COCO	VG-500	VOC-2007
ML-AGCN (A)	81.1	17	94.27
ML-AGCN (A+B)	86.6 (+5.1%)	37.5 (+20.5%)	94.31 (+0.04%)
ML-AGCN (A+B+C)	86.7 (0.1%)	37.9 (+0.4%)	94.48 (+0.17%)

different protocols are followed with different combinations of source and target datasets. Two categories of methods are considered in our evaluation: (1) the conventional Multi-Label Image Classification (MLIC); and the Domain Adaptation-based (DA) methods that aim at explicitly reducing the gap between source and target datasets.

Table V reports the results obtained considering AID and UCM datasets. Two different settings are considered: AID \rightarrow UCM, where AID is the source dataset and UCM is the target dataset, and UCM \rightarrow AID, where UCM is the source dataset and AID is the target dataset. It can be clearly seen, in both types of DA settings, that the proposed DA-AGCN outperforms existing state-of-the-art methods in terms of mAP while requiring a lower number of parameters. More specifically, an improvement of mAP by 10.65% and 4.59% has been respectively recorded for AID \rightarrow UCM and UCM \rightarrow AID in terms of mAP as compared with the DA-MAIC [22]

baseline. This suggests that learning the graph topology in an end-to-end manner helps improve the performance in the presence of a domain shift.

In Table VI, DA-AGCN is also compared with existing methods by considering the settings UCM \rightarrow DFC and AID \rightarrow DFC. It can be remarked that DA-AGCN outperforms the existing works in terms of mAP and model size for UCM \rightarrow DFC. However, the performance of our approach is lower than DA-MAIC under the AID \rightarrow DFC setting. But interestingly, the per-class precision (PC), per-class recall (PC), overall recall (OR), and per-class and overall F1-score register a significant improvement compared to the baseline. This indicates that in the presence of class imbalance, our method performs better than the state-of-the-art by a significant margin.

b) *Ablation study*: Table VII reports the obtained mAP when considering each module of DA-AGCN. The results confirm that adding both an AGCN subnet and an adversarially trained domain classifier (DC) enhances the performance. Additionally, in Table VIII, the performance when discarding the proposed adjacency matrices B and C is reported for the four settings. The obtained results confirm the relevance of using the proposed attention-based and similarity-based adjacency matrices for modeling label correlations.

TABLE V: Comparison with the state-of-the-art in terms of mAP and number of model parameters using two settings, i.e., AID \rightarrow UCM and UCM \rightarrow AID. (Best performance is indicated in bold).

Category	Method	# params	AID \rightarrow UCM							UCM \rightarrow AID						
			mAP	CP	CR	CFI	OP	OR	OFI	mAP	CP	CR	CFI	OP	OR	OFI
MLIC	DELTA [30]	134.7	26.16	15.23	28.79	19.92	47.48	54.69	50.83	31.83	34.46	15.13	20.64	51.02	34.65	41.27
	KSSNET [9]	44.9	20.89	12.32	24.89	16.48	50.79	55.31	50.79	26.45	7.12	9.22	8.03	58.84	24.87	34.97
	TRESNET [6]	53.8	37.03	29.6	34.04	31.33	48.45	69.59	57.13	33.98	15.97	17.66	16.77	54.80	36.09	43.52
	ASL [24]	53.8	12.33	16.15	30.46	21.11	38.26	79.25	51.61	39.79	53.27	31.06	39.24	78.79	44.99	57.28
DA	CDAN [20]	61.0	39.31	48.92	21.72	30.08	80.94	44.24	57.21	39.31	48.92	21.72	30.08	80.94	44.24	57.21
	MCD [31]	44.6	40.57	47.39	16.61	26.36	73.37	31.7	45.59	38.00	30.67	18.11	22.77	80.69	35.31	49.12
	DA-MAIC [22]	44.9	45.51	48.76	43.78	46.13	74.08	80.65	77.23	51.21	59.08	36.66	45.25	82.94	65.08	72.93
Ours	DA-AGCN	35.9	56.16	49.25	52.94	47.72	58.15	80.30	67.45	55.80	59.14	34.14	40.18	88.00	56.53	68.84

TABLE VI: Comparison with the state-of-the-art in terms of mAP and number of model parameters using two settings, i.e., UCM \rightarrow DFC and AID \rightarrow DFC. (Best performance is indicated in bold).

Category	Method	# params	UCM \rightarrow DFC							AID \rightarrow DFC						
			mAP	CP	CR	CFI	OP	OR	OFI	mAP	CP	CR	CFI	OP	OR	OFI
MLIC	DELTA [30]	134.7	44.135	19.66	20.16	19.91	38.9	13.36	19.83	51.59	37.75	51.57	43.6	33.8	37.96	35.76
	KSSNET [9]	44.9	42.996	9.22	33.33	14.44	27.57	20.77	23.7	45.17	20.05	38.34	26.33	28.83	24.42	26.44
	TRESNET [6]	53.8	53.773	35.13	17.8	23.63	40.19	16.34	23.23	62.36	44.64	55.54	49.49	32.42	36.55	34.36
	ASL [24]	53.8	61.995	39.49	28.51	33.11	37.83	24.09	29.43	58.26	35.99	40.54	38.13	34.9	37.62	36.21
DA	CDAN [20]	61.0	55.386	25.29	27.84	26.5	35.71	24.48	29.05	57.53	36.65	51.87	44.94	31.67	33.91	32.75
	MCD [31]	44.6	43.561	19.19	18.97	19.08	27.8	23.86	25.68	44.41	22.04	50.48	30.69	28.56	32.23	30.28
	DA-MAIC (da-maic)	44.9	68.663	42.28	33.55	37.41	43.85	25.44	23.86	72.99	46.18	59.62	52.05	46.12	42.73	44.36
Ours	DA-AGCN	35.9	76.488	65.87	65.8	59.79	57.7	64.69	60.99	65.6	49.97	82.4	57.08	43.95	84.64	57.85

TABLE VII: Ablation study: impact of using and adversarial strategy and learning an adaptive graph topology learning.

Methods/Dataset (mAP)	UCM \rightarrow AID	AID \rightarrow UCM	AID \rightarrow DFC	UCM \rightarrow DFC
TResNet only	34.98	37.03	62.36	54.77
TResNet + AGCN	53.62 (+18.64)	53.08 (+16.05)	58.44 (-3.92)	74.4 (+19.68)
TResNet + AGCN + DC	55.79 (+2.17)	55.37 (+2.29)	65.11 (+6.67)	76.49 (+2.04)

TABLE VIII: Ablation study: effect of adaptively learning B and C in the presence of a domain shift.

Methods/Dataset (mAP %)	UCM \rightarrow AID	AID \rightarrow UCM	AID \rightarrow DFC	UCM \rightarrow DFC
A	42.82	33.64	42.56	58.26
A+B	55.35 (+12.53)	45.14 (+11.5)	51.47 (+8.91)	67.86 (+9.6)
A+B+C	55.79 (+0.44)	55.37 (+10.23)	65.11 (+13.64)	76.49 (+8.63)

4) *Qualitative analysis:* Grad-CAM [42] visualization in the presence of a domain shift can be seen in Fig. 6. While Fig. 6a demonstrate these results for UCM \rightarrow AID, Fig. 6b showcases the visualizations for AID \rightarrow UCM. The left-most column is the input image, and the next three consecutive columns represent the Grad-CAM visualization of the image using a model trained with; A, A and B, and A, B, C respectively. It can be clearly seen that adaptively learning the graph topology B and C helps activate the most relevant areas of interest, leading to better classification performance.

5) *Failure cases:* In order to understand the drop in performance obtained for AID \rightarrow DFC, we show some failure cases in Fig. 7 where the Grad-CAM visualization with A, A and B and A, B and C is shown. It can be noticed that when the targeted object occupies most of the image specifically, the use of B and C makes the model confuse the object with the background. A good illustration of this can be seen in the first row of Fig. 7. The water is confused with the background. In future work, modeling the object occupancy will be investigated for handling these failure cases.

VII. CONCLUSION

The use of graphs for modeling label correlations has shown great performance in the context of multi-label image classification. This has been proven initially proven for a single

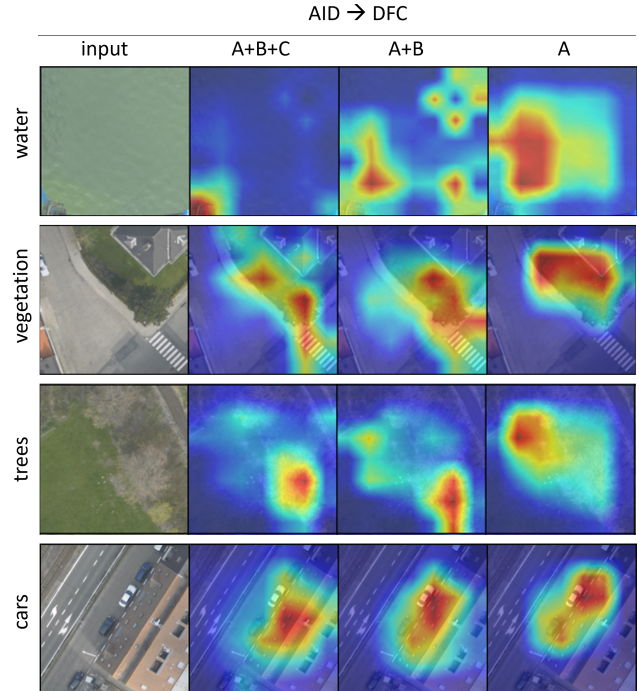


Fig. 7: Failure cases: Grad-CAM visualization for AID \rightarrow DFC showcasing performance degradation with adaptive graphs.

domain. Lately, this has also been demonstrated for multiple domains, which necessitates using an unsupervised domain adaptation strategy. Nevertheless, existing methods mostly fix the graph topology heuristically while discarding edges with rare co-occurrences. Furthermore, it has been demonstrated in [14] that successive GCN aggregations tend to destroy the initial feature similarity. Hence, as a solution, an adaptive strategy for learning the graph in an end-to-end manner is proposed. In particular, attention-based and similarity-preserving

mechanisms are adopted. The proposed framework for multi-label classification in a single domain is then extended to multiple domains. For that purpose, an adversarial domain adaptation strategy is employed. The results performed for both single and multiple domains support the effectiveness of the proposed method in terms of model performance and size as compared to recent state-of-the-art methods.

REFERENCES

- [1] Papadopoulos, K., Ghorbel, E., Aouada, D., and Ottersten, B. (2021, January). Vertex feature encoding and hierarchical temporal modeling in a spatio-temporal graph convolutional network for action recognition. *In 2020 25th International Conference on Pattern Recognition (ICPR)* (pp. 452-458).
- [2] Cai, Y., Ge, L., Liu, J., Cai, J., Cham, T. J., Yuan, J., and Thalmann, N. M. (2019). Exploiting spatial-temporal relationships for 3d pose estimation via graph convolutional networks. *In Proceedings of the IEEE/CVF international conference on computer vision* (pp. 2272-2281).
- [3] Li, Y., Huang, C., Loy, C.C. and Tang, X., 2016, October. Human attribute recognition by deep hierarchical contexts. *In European conference on computer vision* (pp. 684-700). Springer, Cham.
- [4] Shao, J., Kang, K., Change Loy, C. and Wang, X., 2015. Deeply learned attributes for crowded scene understanding. *In Proceedings of the IEEE conference on computer vision and pattern recognition* (pp. 4657-4666).
- [5] Bell, S., Zitnick, C.L., Bala, K. and Girshick, R., 2016. Inside-outside net: Detecting objects in context with skip pooling and recurrent neural networks. *In Proceedings of the IEEE conference on computer vision and pattern recognition* (pp. 2874-2883).
- [6] Ridnik, T., Lawen, H., Noy, A., Ben Baruch, E., Sharir, G., and Friedman, I. (2021). "Tresnet: High performance gpu-dedicated architecture." *In Proceedings of the IEEE/CVF Winter Conference on Applications of Computer Vision* (pp. 1400-1409).
- [7] He, K., Zhang, X., Ren, S., and Sun, J. (2016). Deep residual learning for image recognition. *In Proceedings of the IEEE conference on computer vision and pattern recognition* (pp. 770-778).
- [8] Huang, G., Liu, Z., Van Der Maaten, L. and Weinberger, K.Q., 2017. Densely connected convolutional networks. *In Proceedings of the IEEE conference on computer vision and pattern recognition* (pp. 4700-4708).
- [9] Wang, Y., He, D., Li, F., Long, X., Zhou, Z., Ma, J. and Wen, S., 2020, April. Multi-label classification with label graph superimposing. *In Proceedings of the AAAI Conference on Artificial Intelligence* (Vol. 34, No. 07, pp. 12265-12272).
- [10] Chen, Z.M., Wei, X.S., Wang, P. and Guo, Y., 2019. Multi-label image recognition with graph convolutional networks. *In Proceedings of the IEEE/CVF conference on computer vision and pattern recognition* (pp. 5177-5186).
- [11] Singh, I.P., Oyedotun, O., Ghorbel, E. and Aouada, D., 2022. IML-GCN: Improved Multi-Label Graph Convolutional Network for Efficient yet Precise Image Classification. *In AAAI-22 Workshop Program-Deep Learning on Graphs: Methods and Applications*.
- [12] Pennington, J., Socher, R. and Manning, C.D., 2014, October. Glove: Global vectors for word representation. *In Proceedings of the 2014 conference on empirical methods in natural language processing (EMNLP)* (pp. 1532-1543).
- [13] Velickovic, P., Cucurull, G., Casanova, A., Romero, A., Lio, P. and Bengio, Y., 2017. Graph attention networks. *stat*, 1050, p.20.
- [14] Jin, W., Derr, T., Wang, Y., Ma, Y., Liu, Z. and Tang, J., 2021, March. Node similarity preserving graph convolutional networks. *In Proceedings of the 14th ACM International Conference on Web Search and Data Mining* (pp. 148-156).
- [15] Ganin, Y. and Lempitsky, V., 2015, June. Unsupervised domain adaptation by backpropagation. In International conference on machine learning (pp. 1180-1189). PMLR.
- [16] Li, M., Zhai, Y.M., Luo, Y.W., Ge, P.F. and Ren, C.X., 2020. Enhanced transport distance for unsupervised domain adaptation. *In Proceedings of the IEEE/CVF Conference on Computer Vision and Pattern Recognition* (pp. 13936-13944).
- [17] Zhang, Y., Liu, T., Long, M. and Jordan, M., 2019, May. Bridging theory and algorithm for domain adaptation. *In International Conference on Machine Learning* (pp. 7404-7413). PMLR.
- [18] Long, M., Zhu, H., Wang, J. and Jordan, M.I., 2017, July. Deep transfer learning with joint adaptation networks. *In International conference on machine learning* (pp. 2208-2217). PMLR.
- [19] Ganin, Y., Ustinova, E., Ajakan, H., Germain, P., Larochelle, H., Laviolette, F., Marchand, M. and Lempitsky, V., 2016. Domain-adversarial training of neural networks. *The journal of machine learning research*, 17(1), pp.2096-2030.
- [20] Long, M., Cao, Z., Wang, J. and Jordan, M.I., 2018. Conditional adversarial domain adaptation. *Advances in neural information processing systems*, 31.
- [21] Tang, H. and Jia, K., 2020, April. Discriminative adversarial domain adaptation. *In Proceedings of the AAAI Conference on Artificial Intelligence* (Vol. 34, No. 04, pp. 5940-5947).
- [22] Lin, D., Lin, J., Zhao, L., Wang, Z.J. and Chen, Z., 2021. Multilabel Aerial Image Classification With Unsupervised Domain Adaptation. *IEEE Transactions on Geoscience and Remote Sensing*.
- [23] Pham, D.D., Koesnadi, S.M., Dovletov, G. and Pauli, J., 2021, April. Unsupervised Adversarial Domain Adaptation for Multi-Label Classification of Chest X-Ray. *In 2021 IEEE 18th International Symposium on Biomedical Imaging (ISBI)* (pp. 1236-1240). IEEE.
- [24] Ridnik, T., Ben-Baruch, E., Zamir, N., Noy, A., Friedman, I., Protter, M. and Zelnik-Manor, L., 2021. Asymmetric loss for multi-label classification. *In Proceedings of the IEEE/CVF International Conference on Computer Vision* (pp. 82-91).
- [25] Xia, G.S., Hu, J., Hu, F., Shi, B., Bai, X., Zhong, Y., Zhang, L. and Lu, X., 2017. AID: A benchmark data set for performance evaluation of aerial scene classification. *IEEE Transactions on Geoscience and Remote Sensing*, 55(7), pp.3965-3981.
- [26] Hua, Y., Mou, L. and Zhu, X.X., 2020. Relation network for multi-label aerial image classification. *IEEE Transactions on Geoscience and Remote Sensing*, 58(7), pp.4558-4572.
- [27] B. Chaudhuri, B. Demir, S. Chaudhuri, and L. Bruzzone, "Multilabel remote sensing image retrieval using a semisupervised graph-theoretic method," *IEEE Transactions on Geoscience and Remote Sensing*, vol. 56, no. 2, pp. 1144-1158, 2018.
- [28] Y. Yang and S. Newsam, "Bag-of-visual-words and spatial extensions for land-use classification," in *International Conference on Advances in Geographic Information Systems (SIGSPATIAL)*, 2010.
- [29] Y. Hua, L. Mou, and X. X. Zhu, "Recurrently exploring class-wise attention in a hybrid convolutional and bidirectional LSTM network for multi-label aerial image classification," *ISPRS J. Photogramm. Remote Sens.*, vol. 149, pp. 188-199, Mar. 2019.
- [30] Yu, W.J., Chen, Z.D., Luo, X., Liu, W. and Xu, X.S., 2019. DELTA: A deep dual-stream network for multi-label image classification. *Pattern Recognition*, 91, pp.322-331.
- [31] Saito, K., Watanabe, K., Ushiku, Y. and Harada, T., 2018. Maximum classifier discrepancy for unsupervised domain adaptation. *In Proceedings of the IEEE conference on computer vision and pattern recognition* (pp. 3723-3732).
- [32] Velickovic, P., Cucurull, G., Casanova, A., Romero, A., Lio, P. and Bengio, Y., 2017. Graph attention networks. *stat*, 1050, p.20.
- [33] Lin, T. Y., Maire, M., Belongie, S., Hays, J., Perona, P., Ramanan, D., ... and Zitnick, C. L. (2014, September). Microsoft coco: Common objects in context. *In European conference on computer vision* (pp. 740-755). Springer, Cham.
- [34] Krishna, R., Zhu, Y., Groth, O., Johnson, J., Hata, K., Kravitz, J., Chen, S., Kalantidis, Y., Li, L.J., Shamma, D.A. and Bernstein, M.S., 2017. Visual genome: Connecting language and vision using crowdsourced dense image annotations. *International journal of computer vision*, 123(1), pp.32-73.
- [35] Chen, T., Lin, L., Hui, X., Chen, R. and Wu, H., 2020. Knowledge-guided multi-label few-shot learning for general image recognition. *IEEE Transactions on Pattern Analysis and Machine Intelligence*.
- [36] Everingham, M., Van Gool, L., Williams, C.K., Winn, J. and Zisserman, A., 2010. The pascal visual object classes (voc) challenge. *International journal of computer vision*, 88(2), pp.303-338.
- [37] Lanchantin, J., Wang, T., Ordonez, V. and Qi, Y., 2021. General multi-label image classification with transformers. *In Proceedings of the IEEE/CVF Conference on Computer Vision and Pattern Recognition* (pp. 16478-16488).
- [38] Chen, T., Xu, M., Hui, X., Wu, H. and Lin, L., 2019. Learning semantic-specific graph representation for multi-label image recognition. *In Proceedings of the IEEE/CVF international conference on computer vision* (pp. 522-531).
- [39] Wang, J., Yang, Y., Mao, J., Huang, Z., Huang, C. and Xu, W., 2016. Cnn-rnn: A unified framework for multi-label image classification. *In Proceedings of the IEEE conference on computer vision and pattern recognition* (pp. 2285-2294).
- [40] Ge, W., Yang, S. and Yu, Y., 2018. Multi-evidence filtering and fusion for multi-label classification, object detection and semantic segmentation

- based on weakly supervised learning. *In Proceedings of the IEEE conference on computer vision and pattern recognition* (pp. 1277-1286).
- [41] Singh, I. P., Ghorbel, E., Oyedotun, O., and Aouada, D. (2022). Multi label image classification using adaptive graph convolutional networks (ML-AGCN). *In IEEE International Conference on Image Processing*.
- [42] Selvaraju, R. R., Cogswell, M., Das, A., Vedantam, R., Parikh, D., and Batra, D. (2017). Grad-cam: Visual explanations from deep networks via gradient-based localization. *In Proceedings of the IEEE international conference on computer vision* (pp. 618-626).
- [43] He, T., Zhang, Z., Zhang, H., Zhang, Z., Xie, J., and Li, M. (2019). Bag of tricks for image classification with convolutional neural networks. *In Proceedings of the IEEE/CVF Conference on Computer Vision and Pattern Recognition* (pp. 558-567).
- [44] Xie, S., Girshick, R., Dollár, P., Tu, Z., and He, K. (2017). Aggregated residual transformations for deep neural networks. *In Proceedings of the IEEE conference on computer vision and pattern recognition* (pp. 1492-1500).
- [45] Hu, J., Shen, L., and Sun, G. (2018). Squeeze-and-excitation networks. *In Proceedings of the IEEE conference on computer vision and pattern recognition* (pp. 7132-7141).
- [46] Tan, M., and Le, Q. (2019, May). Efficientnet: Rethinking model scaling for convolutional neural networks. *In International conference on machine learning* (pp. 6105-6114).
- [47] Wei, Y., Xia, W., Lin, M., Huang, J., Ni, B., Dong, J., ... and Yan, S. (2015). HCP: A flexible CNN framework for multi-label image classification. *IEEE transactions on pattern analysis and machine intelligence*, 38(9), 1901-1907.
- [48] Deng, J., Dong, W., Socher, R., Li, L. J., Li, K., and Fei-Fei, L. (2009, June). Imagenet: A large-scale hierarchical image database. *In 2009 IEEE conference on computer vision and pattern recognition* (pp. 248-255).
- [49] Zhu, F., Li, H., Ouyang, W., Yu, N., and Wang, X. (2017). Learning spatial regularization with image-level supervisions for multi-label image classification. *In Proceedings of the IEEE conference on computer vision and pattern recognition* (pp. 5513-5522).
- [50] Thomas N. Kipf, Max Welling, Semi-Supervised Classification with Graph Convolutional Networks (*ICLR 2017*)
- [51] Sharif Razavian, A., Azizpour, H., Sullivan, J., and Carlsson, S. (2014). CNN features off-the-shelf: an astounding baseline for recognition. *In Proceedings of the IEEE conference on computer vision and pattern recognition workshops* (pp. 806-813).
- [52] P. Sermanet, D. Eigen, X. Zhang, M. Mathieu, R. Fergus, and Y. LeCun. Overfeat: Integrated recognition, localization and detection using convolutional networks. *In ICLR, 2014*.
- [53] A. Krizhevsky, I. Sutskever, and G. Hinton, "Imagenet classification with deep convolutional neural networks," in *Proc. Neural Inf. Process. Syst., 2012*, pp. 1106-1114.
- [54] Simonyan, K., Zisserman, A. (2015). Very Deep Convolutional Networks for Large-Scale Image Recognition. *In Y. Bengio and Y. LeCun (Eds.), 3rd International Conference on Learning Representations, ICLR 2015*
- [55] Pham, D. D., Koesnadi, S. M., Dvletov, G., & Pauli, J. (2021, April). Unsupervised Adversarial Domain Adaptation for Multi-Label Classification of Chest X-Ray. *In 2021 IEEE 18th International Symposium on Biomedical Imaging (ISBI)* (pp. 1236-1240).
- [56] Mirza, M., & Osindero, S. (2014). Conditional generative adversarial nets. *arXiv preprint arXiv:1411.1784*.
- [57] Li, G., Ji, Z., Chang, Y., Li, S., Qu, X., & Cao, D. (2021). ML-ANet: A transfer learning approach using adaptation network for multi-label image classification in autonomous driving. *Chinese Journal of Mechanical Engineering*, 34(1), 1-11.
- [58] Qu, X., Che, H., Huang, J., Xu, L., & Zheng, X. (2021). Multi-layered semantic representation network for multi-label image classification. *arXiv preprint arXiv:2106.11596*.



Inder Pal Singh is a PhD student at the Interdisciplinary center for Security, Reliability and Trust (SnT), University of Luxembourg under the supervision of Dr. Djamila Aouada. He completed his Master in Computer Vision from the University of Burgundy, France in 2020. His research interests include machine learning, computer vision and pattern recognition.



Enjie Ghorbel is Research Scientist at the Interdisciplinary center for Security, Reliability and Trust (SnT), University of Luxembourg. She received her engineering diploma from the National Engineering School of Sousse (ENISo) in Applied Computer Science in 2014 and her PhD diploma in Computer Science, from the University of Normandie, in 2017. Her research interests include computer vision and pattern recognition.



Oyebade Oyedotun is currently a Senior Machine Learning Scientist at Spire Global. He received his PhD degree in 2020 from the Interdisciplinary Centre for Security, Reliability and Trust (SnT), University of Luxembourg. His research interests include deep learning, machine learning and vision applications.



Djamila Aouada is Senior Research Scientist and Assistant Professor at the Interdisciplinary Centre for Security, Reliability, and Trust (SnT), University of Luxembourg. She is Head of the Computer Vision, Imaging and Machine Intelligence (CVI2) Research Group at SnT, and Head of the SnT Computer Vision Laboratory and co-Head of the SnT Zero-G Laboratory. Dr. Aouada received the State Engineering degree in electronics in 2005, from the École Nationale Polytechnique (ENP), Algiers, Algeria, and the Ph.D. degree in electrical engineering in 2009 from North Carolina State University (NCSU), Raleigh, NC, USA. Dr. Aouada has worked as a consultant for multiple renowned laboratories (Los Alamos National Laboratory, Alcatel Lucent Bell Labs., and Mitsubishi Electric Research Labs.). She has been leading the computer vision activities at SnT since 2009. Her research interests span the areas of image processing, computer vision, and data modelling. Dr. Aouada is Senior Member of the IEEE, member of the IEEE Signal Processing Society, IEEE WIE, INSTICC and the Eta Kappa Nu honor society (HKN). She has served as the Chair of the IEEE Benelux Women in Engineering Affinity Group from 2014 to 2016, Chair of the SHARP workshop at ECCV 2020, CVPR 2021 and CVPR 2022, Area Chair at 3DV 2020 and 2022 and Program Chair at 3DV 2021, General Chair at RTIP2R 2022, and Program Chair at EUVIP 2023. She is the recipient of four IEEE best paper awards.